Journal of South American Earth Sciences 170 (2026) 105891

Contents lists available at ScienceDirect

Journal of South American Earth Sciences

journal homepage: www.elsevier.com/locate/jsames

Isotope-informed water sources and recharge mechanisms in a tropical karst environment of the Talgua River Basin, Honduras

Jorge Cardona-Hernández [a,b], Germain Esquivel-Hernández [c,*], Lucilena Rebelo Monteiro [d], Ricardo Sánchez-Murillo [e], Marycel E.B. Cotrim [d], Rolando Sánchez-Gutiérrez [c], Christian Birkel [f], Tania Peña-Paz [g], Laura Benegas-Negri [h]

[a] Facultad Ciencias de la Tierra y la Conservación, Universidad Nacional de Agricultura, Catacamas, Honduras
[b] Doctorado en Ciencias Naturales para el Desarrollo, DOCINADE, San José, Costa Rica
[c] Stable Isotopes Research Group and Water Resources Management Laboratory, School of Chemistry, Universidad Nacional, Heredia, Costa Rica
[d] Instituto de Pesquisas Energéticas e Nucleares, São Paulo, Brazil
[e] Department of Earth and Environmental Sciences, University of Texas at Arlington, Arlington, TX, USA
[f] Department of Geography, Water, and Global Change Observatory, University of Costa Rica, San José, Costa Rica
[g] Instituto Hondureño de Ciencias de la Tierra, Universidad Nacional Autónoma de Honduras, Tegucigalpa, Honduras
[h] Centro Agronómico Tropical de Investigación y Enseñanza (CATIE), Turrialba, Costa Rica

ARTICLE INFO

Keywords:
Honduras' karstic systems
Water stable isotopes
D-excess and LC-Excess
Focused recharge mechanism
HYSPLIT

ABSTRACT

Understanding groundwater recharge mechanisms in karst zones is critical for preserving water supply, establishing water-use policies, and monitoring water pollution. In this study, we analyzed the isotope composition (δ^2H and $\delta^{18}O$) of rainfall, surface water, and groundwater in the Talgua River basin in northeastern Honduras between August 2019 and December 2023. The main goal was to study the relationship between rainfall inputs and recharge mechanisms in a complex karstic environment, characterized by high rainfall seasonality and variable land use. The $\delta^{18}O$ and δ^2H relationship in rainfall resulted in a significant local meteoric water line of $\delta^2H = 7.68 \pm 0.08 \cdot \delta^{18}O + 9.47 \pm 0.42$ ($N = 223$, $r^2 = 0.97$, $p < 0.001$). HYSPLIT air mass trajectory and cluster analysis using $\delta^{18}O$ and deuterium excess (*d*-excess) revealed that moisture sources in the Talgua River basin originated mainly from the Caribbean Sea (89 %) with minimal contributions from the Pacific Ocean and the Gulf of Mexico (11 %). Recharge is mainly driven by heavy, isotopically depleted rainfall during the May–November (wet season), as indicated by the rainfall to groundwater (P/GW) $^{18}O/^{16}O$ ratios. *d*-excess and the line-conditioned excess (LC-excess) values indicate substantial meteoric inputs during the wet season, reflecting a recycled-moisture signal that contributes to recharge, with only minor evapoconcentration effects. This study systematically provides essential insights into rainfall, surface water, and groundwater interactions in the poorly understood karstic regions of Central America. It advances our understanding of tropical karst hydrological processes, such as moisture transport and recharge mechanisms, and provides valuable information for water resource evaluation and management.

1. Introduction

Karst aquifers constitute geological formations with complex hydrogeological and lithological characteristics (Bakalowicz, 2005). This heterogeneity is inherent to rock dissolution processes driven by carbonic acid in water, which dissolves carbonate rocks. The decomposition of abundant plant material increases carbon dioxide availability, which then interacts with runoff from heavy rainfall, accelerating karst development (Ensley et al., 2021; Tarbuck et al., 2019). A karst aquifer can be conceptualized as an open system within the catchment, characterized by input, throughput, and output water flows. Even in relatively simple karst aquifers, multiple subsurface systems with limited hydraulic connectivity may coexist, each draining into distinct conduit networks (Ford and Williams, 2007). As a result, mixed flows develop, integrating pathways with highly variable velocities, from very slow to extremely rapid, through large fractures and subterranean channels (Arbel et al., 2010; Guo et al., 2018; White, 2007; Zhang et al., 2019). Karst catchments are often characterized by a thin soil cover,

* Corresponding author. Universidad Nacional Costa Rica Campus Omar Dengo, P.O. Box 86-3000, Heredia, Costa Rica.
E-mail address: germain.esquivel.hernandez@una.ac.cr (G. Esquivel-Hernández).

https://doi.org/10.1016/j.jsames.2025.105891
Received 16 October 2025; Received in revised form 19 November 2025; Accepted 25 November 2025
Available online 27 November 2025

epikarst with high infiltration capacity, and vadose and phreatic zones containing networks of fractures, fissures, and conduits (Jukić et al., 2021; Williams, 2008). In catchments where karst rocks predominate, groundwater recharge is derived from autogenic/diffuse recharge (Ensley et al., 2021; Ford and Williams, 2007). The autogenic/diffuse recharge is related to a major mechanism of groundwater recharge, with water infiltrating through the root and vadose zones via piston flow (Good et al., 2015). However, more complex geological conditions are typically found, and runoff also drains into karst aquifers from adjacent or overlying non-karstic rocks (i.e., allogenic or focused recharge; Li et al., 2024). Overall, karst recharge is predominantly focused through preferential flow paths, with a significant amount of water rapidly entering the aquifer through discrete conduits such as sinkholes, sinking streams, and swallets. In some karst areas (e.g., Loess Plateau, China), focused recharge may contribute to up to ~90 % of total recharge (Li et al., 2017), although equally distributed contributions from diffuse and focused recharge were also reported (Shen et al., 2022). This process is like the diffuse recharge, but the presence of a well-developed network of interconnected conduits and caves accelerates the flow, bypassing the slower piston flow of the vadose zone (Hartmann et al., 2014). Consequently, this rapid infiltration in karst systems can lead to a quick and significant rise in the water table level, making them highly vulnerable to contamination from surface activities (Ding et al., 2020; Jasechko and Taylor, 2015).

Climate patterns across the tropics are changing, with increases in extreme hydrometeorological events and convective rainfall projected over Central America (Giorgi, 2006; Emanuel, 2021; Berg et al., 2013; Fowler et al., 2021). While heavy precipitation events are expected to intensify, they often contribute less to groundwater recharge and may degrade water quality through flooding and erosion. Karst aquifers, characterized by short response times, are particularly sensitive to these changes, making them key systems for assessing the impacts of climate change on groundwater resources (Hartmann et al., 2014; Giese et al., 2025). Observed and projected decreases in long-term karst recharge, ranging from 5 to 23 % in Israel (Bresinsky et al., 2023; Hepach et al., 2024) to up to 75 % in Spain (Jódar et al., 2025), underscore the need for detailed investigations in tropical karst environments, such as those in northeastern Honduras, where recharge mechanisms remain poorly understood compared to better-studied groundwater systems in Honduras (e.g., Choluteca basin; García-Santos et al., 2021). Based on reported data, sedimentary rock formations cover approximately 40 % of the territory of Honduras, with limestone areas accounting for about ~8 % of the country's total area (Ochoa-Alvarez et al., 1989). Karst aquifers in the Olancho Department of northeastern Honduras could supply water resources for a population of up to 500,000 people. Stable water isotopes provide a powerful tool to disentangle these recharge processes and improve groundwater management under changing climatic conditions. Here, we present a study in the Talgua River basin in northeastern Honduras, a region with a prominent karst landscape and a complex hydrological setting shaped by high rainfall seasonality and diverse land use, including primary forest, coffee plantations, and degraded pastures, all influencing infiltration and runoff dynamics (Hanson et al., 2004; Saravia-Maldonado et al., 2024). This heterogeneity, particularly the contrasting infiltration capacities of degraded pastures versus forested areas, underscores the need for improved understanding of rainfall-runoff generation and groundwater recharge processes. The specific objectives of this study are to determine.

i) the contributions of different tropical moisture sources (e.g., Caribbean Sea, Pacific Ocean, recycled moisture) to rainfall generation in northeastern Honduras;
ii) the main groundwater recharge mechanisms (i.e., diffuse vs. focused recharge contributions) in the karst environment of the Talgua River basin.

We hypothesize that the strong seasonality of precipitation in the Talgua River basin biases groundwater recharge toward the peak rainy season, with recharge further influenced by recycled moisture inputs and evaporation effects driven by land use, karst structures, and the climatic conditions of northeastern Honduras. Our study provides information to further evaluate groundwater recharge under a changing climate (specifically, the intensification of heavy precipitation events) in tropical karstic environments. Even though previous assessments (e.g., Jasechko and Taylor, 2015) indicated that groundwater resources in the tropics are likely to be a climate-resilient source of freshwater, stable isotope-based studies in Central America (Sánchez-Murillo et al., 2020) have highlighted the highly dynamic cycling of mass and energy produced by complex land-ocean-atmosphere interactions, even in this relatively small region. These findings underscore the relevance of studying new areas like the Talgua River basin, which is affected by human interventions and strong seasonal changes in total precipitation volume.

2. Materials and methods

2.1. Study area

Honduras is considered the second most cave- and karst-rich country in Central America, after Guatemala. Karst systems of Honduras are formed by a combination of typical exokarstic structures like sinkholes, cenotes, mogotes (isolated hills), and towers, and best-known endokarstic structures such as caves and caverns (Jeannin et al., 2025; Ulloa et al., 2011). The Atima formation (middle Cretaceous) is considered the most widespread carbonate unit in the country, extending from the western border with Guatemala to the eastern border with Nicaragua. This system houses the main karst areas, including the Susmay Caves, the Río Talgua Caves, the Río Atima sinkhole, as well as the underground drainage of the Río Zacapa with an estimated length >9 km. To a lesser extent, the limestone formation called Jaitique (Cenomanian and late Cretaceous) also hosts many cave systems, among which are the Taulabé Caves and the Siete Quebradas Cave, the second longest in Honduras (Finch and Pistole, 2011).

Our research was conducted in the Talgua River basin, located in the southwestern part of the Sierra de Agalta National Park, northeastern Honduras (Fig. 1a). The basin covers an area of 85.3 km^2 and belongs to the Patuca River basin, which drains to the Caribbean Sea. The Talgua River basin has an average slope of 13.7 %, with elevations ranging from 550 to 2190 m a.s.l. (Fig. 1b and c). In the headwaters, there are three low order streams: Agua, Seco, and Pinabetal (Fig. 1c). Overall, the hydrographic network has a dendritic morphology composed of streams and sub-surface rivers (Saravia-Maldonado et al., 2024). The lithology of the upper area consists of sedimentary rocks like limestone, marl, dolomite, and calcareous rocks from the Cretaceous and Quaternary periods (e.g., Yojoa Group), overlain by shallow dark brown Rendzina clay. The lower basin, which drains into the Olancho Valley, consists of Quaternary-period continental and marine sediments (Dixon et al., 1998; Michelle-Warner, 2016). Soils are well-drained and formed over limestone or marble. Rock outcrops and cliffs are frequent, and they are located on steep terrain with slopes greater than 60 %.

On the northeastern bank of the Talgua river lies the Talgua Caves, a cavern system developed within the Atima Formation, a mid-Cretaceous (Aptian-Albian) carbonate unit that extends from the Guatemalan border in the west to the Nicaraguan border in the east. (Finch and Pistole, 2011). These karst zones are related to the occurrence of subterranean rivers, which disappear or emerge from the catchment slopes, with flows reaching up to 2 m^3/s (Reyes-Sandoval and Serrano-Rodríguez, 2021. Fig. 1d). In the Talgua River basin, most groundwater resources comprise moderately to highly productive local aquifers compared to other groundwater systems in Honduras (60–80 m^3/min, Ochoa-Alvarez et al., 1989). These characteristics are translated into abundant water resources for agricultural activities in the lower valley. In the altitudinal gradient of the Talgua River basin, land use consists of

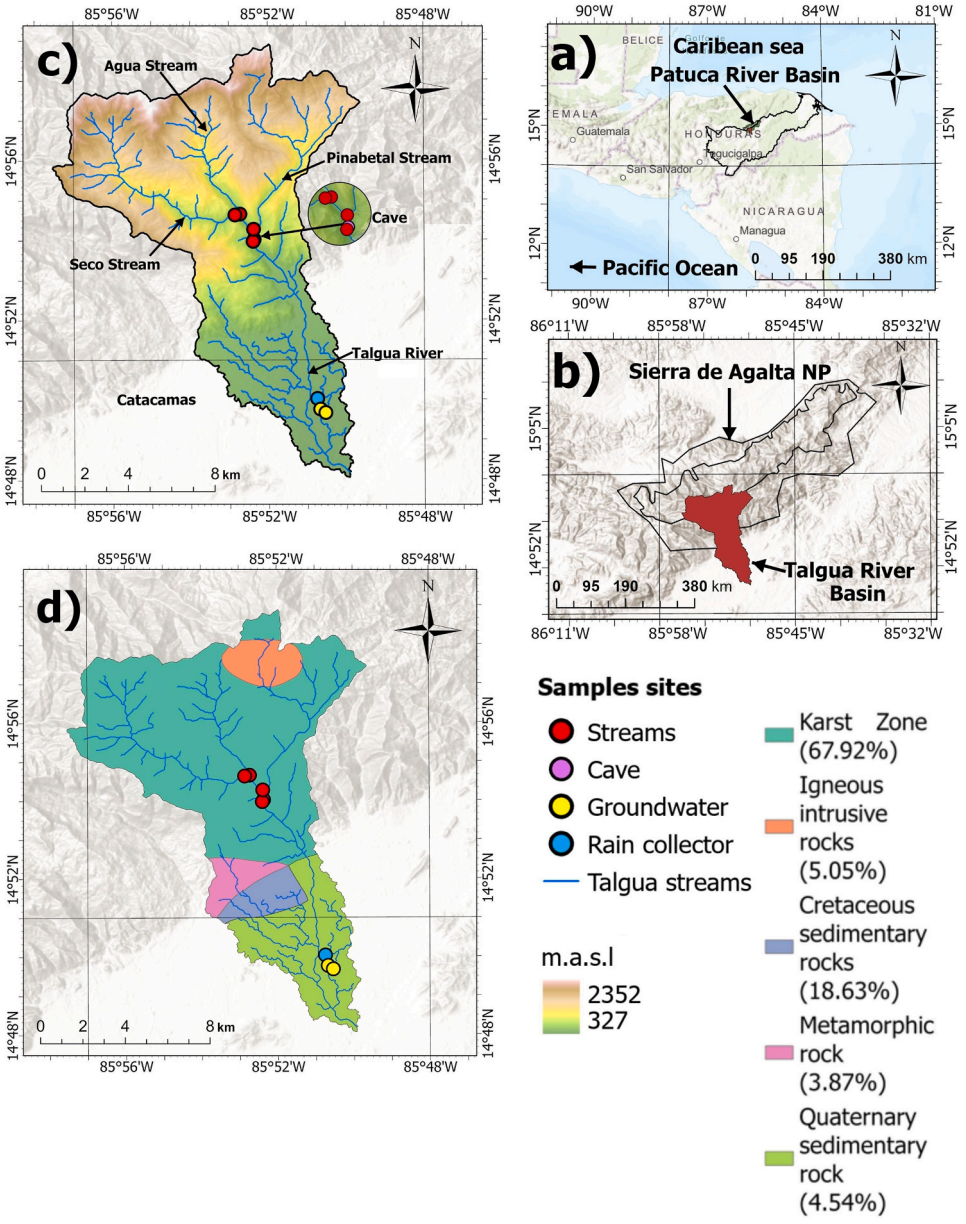

Fig. 1. a) Geographic location of the Patuca basin in northeastern Honduras, Central America. b) Location of the Talgua River basin and the Sierra de Agalta National Park in the Patuca basin. c) The elevation profile of the Talgua River basin (in m a.s.l.) including the corresponding stream network (blue lines). Sampling sites for stream water (red circles), cave infiltration (purple circle), groundwater (yellow circles), and precipitation (blue circle) are also shown. d) Main lithological characteristics of the Talgua River basin showing the area of karst phenomena (~60 %, 51.2 km^2). Land use consists of forest cover (72 %, 61.4 km^2), pastureland, and crops (21 %, 17.9 km^2), with lesser urbanized areas near the municipality of Catacamas (Olancho Department). (For interpretation of the references to color in this figure legend, the reader is referred to the Web version of this article.)

forest cover (72 %), pastureland, and crops (21 %), with lesser urbanized areas near the municipality of Catacamas (Olancho Department). In the mid-to-lower section, the vegetation cover has been cleared for cattle ranching and subsistence farming. In the upper part, the soil is covered by broadleaf forest with agricultural frontier areas that have been cleared to establish coffee farms (Reyes-Sandoval and Serrano-Rodríguez, 2021).

The climate of northeastern Honduras (tropical wet and dry/savanna climate, Aw; Kottek et al., 2006) is characterized by a moisture inflow controlled by cold fronts and trade winds from the Caribbean and Gulf of Mexico in an east-to-west prevailing direction, from December until the onset of the rainy season in April–May. In July and August, the mid-summer drought (also known as 'Canícula') reduces rainfall over the region. Then, from September to November, the Intertropical Convergence Zone (ITCZ) activity and tropical eastern waves, along with the most intense period of the hurricane season, greatly contribute to the moisture input and rainfall generation (García-Santos et al., 2021; Sánchez-Murillo et al., 2019, 2020). The annual rainfall is ~1300 mm/year and ambient air temperature varies between 22 °C and 28 °C throughout the year (Fig. 2). The climate is characterized by well-defined dry and wet periods, resulting in the presence of very humid subtropical and low montane subtropical (Saravia-Maldonado et al., 2024) biomes.

2.2. Sampling methodology

Rainfall stable isotopes data were composed of daily samples (N = 223), collected between August 2019 and December 2023. We extended

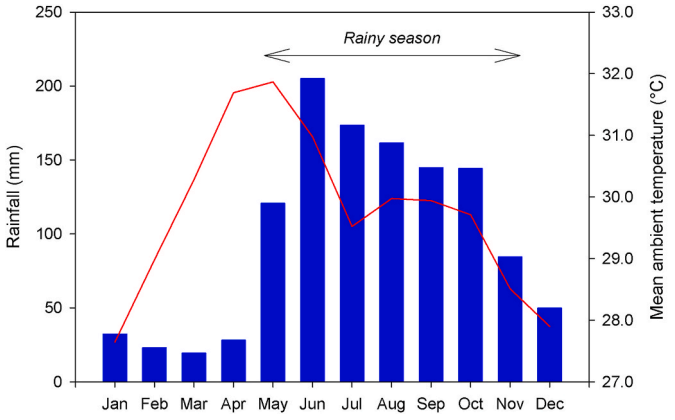

Fig. 2. Climograph showing the monthly mean precipitation (MMP, blue bars) and monthly mean temperature (MMT, red line) for Catacamas. Mean values for both variables were calculated using records available at the Civil Aeronautics Agency of Honduras (2004–2024). (For interpretation of the references to color in this figure legend, the reader is referred to the Web version of this article.)

our rainfall sampling period with respect to the surface and groundwater sampling duration to estimate the local meteoric water line (LMWL) for the Talgua River basin. Rainfall samples were collected using a passive rainfall collector (Palmex Ltd., Croatia; Gröning et al., 2012) installed at 362 m a.s.l (Latitude: 14.834°, Longitude: 85.846°). Due to logistical and security limitations preventing access to a sampling location at the Talgua River headwaters, rainfall samples were only collected at Universidad Nacional de Agricultura in Catacamas. Thus, our study was carried out under the assumption that Catacamas rainfall isotopic data, while altitudinal offset, still provides representative regional data input for our analysis. Rainfall samples were collected every morning at 07:00 (−06:00 GMT) to minimize the risk of isotopic alteration before analysis, particularly in samples exhibiting a high water-to-air ratio in the Palmex bottle or those subject to high ambient temperatures.

Surface water and groundwater samples were collected across an elevation gradient from ~350–600 m asl to capture the isotopic variability throughout different land uses and karst-dominated areas in the Talgua River basin (Fig. 1d). Weekly samples were collected in surface and groundwater reservoirs within the Talgua River basin between September 2020 and February 2023. However, monthly sampling was conducted during the dry season due to the intermittence of some streams in the Talgua River basin. Surface water samples were manually collected at four sampling points along an altitudinal transect: i) Pinabetal (N = 75, Latitude: 14.905°, Longitude: 85.873°, 519 m a.s.l.), ii) Seco (N = 79, Latitude: 14.910°, Longitude: 85.881°, 582 m a.s.l.), iii) Agua (N = 77, Latitude: 14.911°, Longitude: 85.879°, 566 m a.s.l.), and iv) the Talgua river (N = 181, Latitude: 14.899°, Longitude: 85.873°, 494 m a.s.l.). Groundwater samples were collected from two wells (N = 14, 5 m depth, Latitude: 14.829°, Longitude: 85.845°, 357 m a.s.l. and N = 10, 22 m depth, Latitude: 14.828°, Longitude: 85.842°, 354 m a.s.l.). Given the average water table depth in the Talgua River basin (5 m), the 5 m well was classified as shallow groundwater and the 22 m well as deep groundwater. We also collected water samples of the karst infiltration in a closed cavern system (hereafter cave infiltration, N = 107, Latitude: 14.900°, Longitude: 85.873°, 503 m a.s.l.). We consider this karst infiltrating water as a proxy the water entering the phreatic zone through the soil profile and the carbonate bedrock and a good indicator of high and fast infiltration capacity of the thin soil cover and the epikarst (Jukić et al., 2021; Williams, 2008). Precipitation amount was continuously monitored using a weather station installed at the Civil Aeronautics Agency of Honduras (Latitude: 14.838°, Longitude: 85.873°, 391 m a.s.l.) under the administration of National Center for Oceanographic, Atmospheric, and Seismic Studies (CENAOS) and the Permanent Contingency Committee (COPECO). Weather variables were available at 30-min resolution between January 2004 and November 2024. We used this extended 20-year record period to perform a robust characterization of the long-term climate conditions for the Talgua River basin.

2.3. Laboratory analysis

Samples were analyzed at the Stable Isotopes Research Group laboratory at Universidad Nacional (Heredia, Costa Rica) using an IWA-45EP water analyzer (Los Gatos Research, Inc., California, USA) with a precision of ±0.80 ‰ for δ^2H and ±0.08 ‰ for $\delta^{18}O$ (1σ; 5 injections). Isotopic reference materials (RMs), USGS45 ($\delta^2H = -10.30 \pm 0.4$ ‰, $\delta^{18}O = -2.238 \pm 0.011$ ‰; US Geological Survey, Reston, VA, USA), USGS47 ($\delta^2H = -150.2 \pm 0.5$ ‰, $\delta^{18}O = -19.80 \pm 0.02$ ‰; US Geological Survey, Reston, VA, USA), and secondary standard PGW ($\delta^2H = -52.64 \pm 0.26$ ‰, $\delta^{18}O = -8.196 \pm 0.080$ ‰) were used to normalize the results as well as to assess the quality and drift control procedures. Each RM was measured in duplicate at the beginning and at the end of each daily group of analyses. $^{18}O/^{16}O$ and $^2H/^1H$ ratios are presented in delta notation δ (‰ or parts per thousand), relative to the VSMOW-SLAP scale (Skrzypek et al., 2022). Long-term δ^2H and $\delta^{18}O$ precisions are 0.29 ‰ and 0.08 ‰, respectively. The deuterium excess was calculated as $d\text{-excess} = \delta^2H - 8{\cdot}\delta^{18}O$ (Dansgaard, 1964). The line-conditioned excess (LC-excess) was calculated using the LMWL as a reference (Landwehr and Coplen, 2006). The LC-excess is defined as follows:

$$lc\text{-}excess = \delta^2H - ax\delta^{18}O - b \quad (1)$$

where a and b represent the slope and intercept of the LMWL. The uncertainties of d-excess and LC-excess are 0.65 ‰ and 0.68 ‰, respectively. These values were estimated based on the precision of the isotope analysis and slope of the LMWL (Froehlich et al., 2001; Liu et al., 2022).

2.4. HYSPLIT backward trajectories

We computed backward trajectories up to 72 h prior to the precipitation events using the Hybrid Single Particle Lagrangian Integrated Trajectory (HYSPLIT) with Global Data Assimilation System (GDAS) 1° input data (Stein et al., 2015). Air mass trajectory analysis was carried out between August 2019 and November 2022 to analyze the atmospheric conditions prevailing during the dry and wet season conditions. The 72 h-time window was selected to estimate representative moisture transport history with an acceptable accuracy. We followed a two-step process for the trajectory calculations (Fleming et al., 2012): First, fixed endpoint heights between 500 and 2500 m above ground were assessed and in a second step a linear model of their vertical levels against air temperature was used to interpolate and identify the 0 °C isotherm (i.e., the level where precipitation is expected to be formed). To decrease the trajectories' uncertainties and improve the interpretation, given the absence of available information regarding the cloud base height for our study site, a total of 510 trajectories were calculated for 170 rain events at three different heights (700, 1,000, and 2500 m above ground). It is worth noting that our backward trajectory analysis was carried out during a study period was mostly featured by La Niña and neutral conditions.

2.5. Data analysis

We used the k-means algorithm to perform a cluster analysis using the HYSPLIT backward trajectories. The clustering process was applied to identify trajectories with similar geographical origins and to investigate if a similar origin could have significantly influenced the isotopic composition of precipitation. Each cluster has a center (centroid) that is the mean value of all the points in that cluster. K-means locates centers through an iterative procedure that minimizes distances between indi-

vidual points in a cluster and the cluster center. Lloyd's algorithm with squared Euclidean distances was applied to compute the k-means clustering for each k. The Calinski-Harabasz criterion was used to assess optimal number of clusters (Sadeghi, 2025). The Calinski-Harabasz criterion is defined as:

$$\frac{SSB}{SSW} \times \frac{N-k}{k-1} \quad (2)$$

where, SSB is the overall cluster variance, SSW is the within groups cluster variance, K is the number of clusters, and N is the number of observations (170 sampling dates/events at three altitudes in a total of 510 trajectories). The selected variables for cluster analysis were ΔLat (final latitude of trajectory-latitude of sampling point), ΔLong (final longitude of trajectory-longitude of sampling point), the trajectory angle defined as α = arctan(ΔLong/ΔLat), the trajectory altitude (meters above the ground), and a Boolean parameter, Signal (ΔLong), was defined as ΔLong>0. Overall, selected algorithm picked the number of clusters corresponding to the first local maximum of the Calinski-Harabasz index. Thus, k-means algorithm was run for up to 25 clusters if the first local maximum of the index was not reached for a smaller value of k. The smaller number of k was the optimized number of clusters identified with our method. Cluster analysis of trajectories classified the moisture inputs with an error of 1 degree of latitude and 2 degrees of longitude.

Kruskal-Wallis non-parametric one-way analysis of variance on ranks (Kruskal and Wallis, 1952) followed by the Dunn's method (Dunn, 1961) was used to assess differences in the trajectory cluster. As for the isotopic values (i.e., $\delta^{18}O$, *d*-excess, and LC-excess) of water types, pairwise comparisons were performed using the Dunn test and a Bonferroni correction for multiple testing. We used simple linear regression analysis (i.e., ordinary least squares or OLS) to construct the LMWL of the study area (Craig, 1961). The slope and intercept of the LMWL are reported with the corresponding standard errors. These parameters of the LMWL were also used to identify the departure from equilibrium conditions and the effect of kinetic fractionation processes in the isotopic composition of rainfall. The rainfall amount-weighted LMWL for the Talgua River basin was also calculated for comparison (Hughes and Crawford, 2012).

We evaluated groundwater recharge mechanisms using the empirical relationship between rainfall and groundwater isotopic ratios (i.e., P/GW isotopic ratios, Jasechko and Taylor, 2015). To better interpret these P/GW isotopic ratios, the isotopic composition of rainfall and groundwater were expressed in parts per million (ppm) of $^{18}O/^{16}O$ with respect to the Vienna Standard Mean Ocean Water (VSMOW) based on the delta notation definition:

$$\delta^{18}O = \left(\frac{\left(\frac{18_O}{16_O}\right)_{sample}}{\left(\frac{18_O}{16_O}\right)_{VSMOW}} - 1 \right) * 1000 \quad (3)$$

Here, $(^{18}O/^{16}O)_{VSMOW}$ is defined as 0.0020052 (Camin et al., 2025). Given the significant linear relationship between $\delta^{18}O$ and $\delta^{2}H$, the empirical relationship was only evaluated using $^{18}O/^{16}O$ ratios (Sánchez-Murillo and Birkel, 2016).

To quantify relative seasonal contributions of diffuse and focused recharge in the Talgua River basin, we applied a single isotope mass balance based on LC-excess as follows:

$$lc\text{-}ex_{GW} = f_{DR} x lc\text{-}ex_{cave} + f_{FR} x lc\text{-}ex_{rainfall} \quad (4)$$

where f_{DR} and f_{FR} are the fractions of diffuse recharge from deep soil water (i.e., cave infiltration) and focused recharge directly from precipitation to groundwater (%), respectively (Li et al., 2024; Xiang et al., 2019). In Equation (4), lc-ex_{GW}, lc-ex_{cave}, and lc-$ex_{rainfall}$ are the LC-excess of groundwater, cave infiltration (i.e., which mostly comprises the soil cover, the epikarst and the vadose zone; Jukić et al., 2021), and rainfall, in that order. We assume that cave infiltration mostly reflects diffuse recharge slowly entering the phreatic zone through the soil cover and the fracture and matrix permeability of the underlying carbonate bedrock. Under the assumption that $f_{DR} + f_{FR} = 1$ and lc-$ex_{rainfall}$ ~0, the fraction of diffuse recharge (%) was estimated using the following equation (Li et al., 2024):

$$f_{DR} = \frac{lc\text{-}ex_{GW}}{lc\text{-}ex_{cave}} \quad (5)$$

The calculations of f_{DR} and f_{FR} are reported with the corresponding probable error range (PER). The relative errors of lc-ex_{GW} and lc-ex_{SW}, estimated as one standard deviation, were combined using the root mean square method (Topping, 1972).

3. Results

3.1. Isotopic temporal variability in rainfall, surface waters, and groundwater

As for most years in northeastern Honduras, ambient temperatures showed small monthly variations (Fig. 2) with a mean annual temperature of 29.8 ± 1.4 °C estimated for the period 2004–2024. Rainfall was unevenly distributed throughout this study period, and a strong seasonality was recorded (Figs. 2 and 3d). A mean annual precipitation (MAP) of 1187 ± 587 mm was registered, of which 87 % occurred between May and November (Fig. 3d). The local meteoric water line (LMWL) estimated for the Talgua River basin was described as: $\delta^{2}H = 7.68 \pm 0.08 \cdot \delta^{18}O + 9.47 \pm 0.42$ ($r^2 = 0.97$, $p < 0.001$, Fig. 3a). The rainfall amount-weighted LMWL was very similar: $\delta^{2}H = 7.56 \pm 0.07 \cdot \delta^{18}O + 9.17 \pm 0.41$, $r^2 = 0.99$, $p < 0.001$). As for groundwater and surface waters, linear relationships between $\delta^{18}O$ and $\delta^{2}H$ showed slopes <8 and intercepts <10. The smallest slope and intercept were estimated for groundwater (Fig. 3a). The mean $\delta^{18}O$ value of rainfall was −2.77 ‰ and varied from −14.81 ‰ to 3.65 ‰ (Table 1 and Fig. 3b). Mean $\delta^{18}O$ values of groundwater and surface waters were −5.71 ‰ and −5.93 ‰, and fluctuated from −6.72 ‰ and −3.32 ‰ and from −10.67 ‰ and 3.05 ‰, respectively (Fig. 3c).

Overall, rainfall isotope composition (i.e., $\delta^{18}O$) exhibited a bimodal pattern (W-shaped type) throughout the year (Fig. 3e). Significant variations were recorded during the rainiest period (August to October) related to low excursions with $\delta^{18}O$ values up to ~ −15 ‰. Damped temporal variations were also recorded in surface waters and groundwater. Nonetheless, the seasonal variations with respect to the mean $\delta^{18}O$ value estimated for September 2020 and February 2023 was greater in groundwater than in surface waters, mostly during the dry season (December–April) and the mid-summer drought. Significant short-term variations in the isotopic composition of rainfall, surface waters, and groundwater were also evident during the passage of tropical cyclones (e.g., Hurricane Eta and Iota in November 2020 (Fig. 3e). Mean *d*-excess in rainfall was 10.37 ‰ and fluctuated between −8.53 ‰ and 22.60 ‰ (Fig. 3f). *d*-excess was slightly higher in the dry season (11.51 ‰) than the rainy season (9.93 ‰). The LC-excess values showed greater variations in surface waters than in groundwater and systematically followed the precipitation inputs with higher LC-excess values during the wet season and lower LC-excess values during the dry season. Unlike the $\delta^{18}O$ values variations in both water types, seasonal variations with respect to the average LC-excess was greater in surface waters than in groundwater.

3.2. Air mass back trajectory provenance

The air mass back trajectories within the study area are shown in Fig. 4a. Cluster analysis allowed us to classify the atmospheric moisture inputs to the Talgua River basin into two categories: long-range Caribbean air masses (Clusters A and B, ~89 % frequency, Fig. 4a) and short-

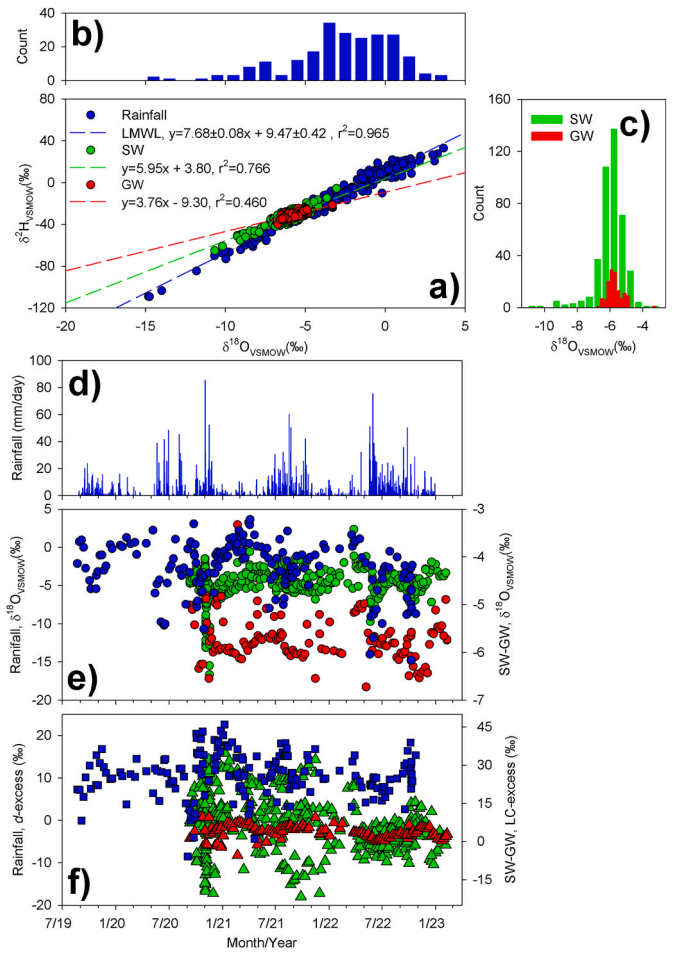

Fig. 3. a) Dual plot of $\delta^{18}O$ (in ‰ relative to the Vienna Standard Mean Ocean Water or VSMOW) versus $\delta^{2}H$ (in ‰ relative to the Vienna Standard Mean Ocean Water or VSMOW) in precipitation (blue circles), surface water (green circles), and groundwater (red circles). The local meteoric water line (LMWL) for the Talgua River basin and the $\delta^{18}O$ and $\delta^{2}H$ linear relationships for surface water and groundwater are also reported. Histograms showing the $\delta^{18}O$ values of rainfall (top panel), surface water and groundwater (right panel) are also shown. b) Time series showing the temporal variation of rainfall (in mm/day) at Talgua River basin between August 2019 and December 2022. c) Time series showing the temporal variation of $\delta^{18}O$ (in ‰) in precipitation (blue circles), surface water (green circles), and groundwater (red circles). d) Time series showing the temporal variation of *d*-excess (in ‰) in rainfall (blue squares) and LC-excess in surface water (green triangles) and groundwater (red triangles). (For interpretation of the references to color in this figure legend, the reader is referred to the Web version of this article.)

range air masses from the Gulf of Mexico basin, the Yucatan Peninsula, and the Pacific Ocean (Clusters C and D, ~11 % frequency, Fig. 4a). $\delta^{18}O$ and *d*-excess values of the Caribbean-sourced moisture were significantly higher at $p < 0.05$ (~2 ‰ and ~10 ‰, respectively, Fig. 4a) than the corresponding $\delta^{18}O$ (~-4 ‰ to −5 ‰) and *d*-excess (~13 ‰–15 ‰) values of short-range air masses (Fig. 4a). As for dry season and wet season conditions, long-range Caribbean air masses also prevailed over the short-range air masses (Clusters A and B, 88–90 % frequency, Fig. 4b and c). However, seasonal $\delta^{18}O$ and *d*-excess values exhibited no statistically significant differences among the clusters during either the dry or wet season ($p > 0.05$).

3.3. Spatial variations in surface water and groundwater isotopic composition

A comparison between $\delta^{18}O$ values, *d*-excess, and LC-excess in

Table 1
Summary of isotope parameters of rainfall, streams and groundwater samples collected in the Talgua River basin, northeastern Honduras.

	$\delta^{18}O$ (‰)						*d*-excess (‰)					LC-excess (‰)				
Sample type	N[a]	Average	Median	Min[b]	Max[c]	SD[d]	Average	Median	Min	Max	SD	Average	Median	Min	Max	SD
Rainfall	223	−2.77	−2.53	−14.81	3.65	3.33	10.37	10.37	−8.53	22.60	4.96	–	–	–	–	–
Pinabetal stream	75	−5.72	−5.78	−6.88	−4.45	0.44	15.04	8.42	2.25	21.64	15.04	3.47	3.67	−2.76	10.09	2.21
Seco stream	79	−5.63	−5.77	−7.88	−3.05	0.74	15.59	7.85	3.04	22.87	15.59	3.79	4.14	−3.11	11.26	2.94
Agua stream	77	−5.87	−5.89	−6.95	−5.03	0.34	16.36	10.72	2.13	21.35	16.36	5.12	5.06	−0.49	9.84	2.10
Talgua river	181	−6.19	−6.09	−10.67	−3.65	1.04	16.70	16.41	8.59	23.52	3.77	5.26	5.10	−2.51	11.92	3.60
Deep groundwater	10	−5.21	−5.29	−5.73	−4.88	0.30	12.21	10.20	2.06	16.66	12.21	1.21	0.70	−1.25	4.99	1.97
Shallow groundwater	14	−5.57	−5.33	−5.77	−4.82	0.37	13.87	8.86	2.42	15.10	13.87	0.74	2.21	−2.52	3.40	2.29
Cave infiltration	107	−5.80	−5.85	−6.72	−3.32	0.45	15.62	5.10	2.58	21.18	15.62	4.16	4.24	−5.43	9.72	2.49

[a] Number of samples.
[b] Minimum.
[c] Maximum.
[d] Standard deviation.

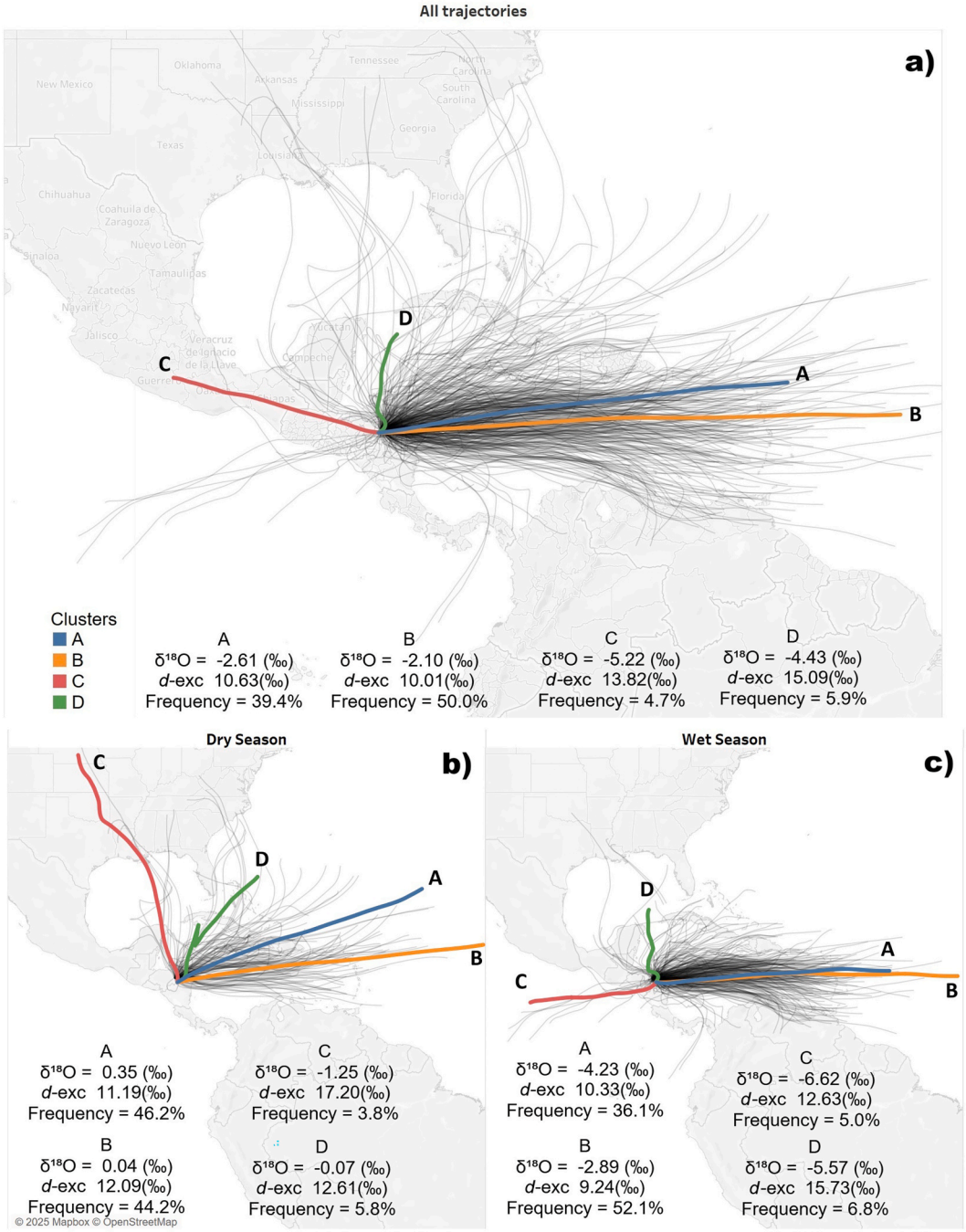

Fig. 4. a) HYSPLIT backward trajectories (72 h) and clustering analysis for Talgua River basin. Black lines denote all air mass back trajectories (N = 170 at three different heights of 700, 1000, and 2500 m above ground) during the sampling period used for the spatial clustering analysis. Mean trajectory clusters (A–D) are color-coded. For each cluster, mean $\delta^{18}O$, *d*-excess and frequency are also reported. b) and c) HYSPLIT backward trajectories (72 h) and clustering analysis for dry season (N = 51) and wet season (N = 119), respectively. (For interpretation of the references to color in this figure legend, the reader is referred to the Web version of this article.)

rainfall, surface water, groundwater, and cave infiltration is shown in Fig. 5 and Table 1. This evaluation was useful to contrast the spatial partitioning of the rainfall input into the surface water and groundwater systems. Mean $\delta^{18}O$ values of Pinabetal, Seco, and Agua streams (i.e., headwaters) were ~ −5 ‰. In the Talgua river, the mean $\delta^{18}O$ value was −6.19 ‰ (Table 1). The range of $\delta^{18}O$ values were similar in the headwaters and the Talgua river with values between −10.67 ‰ and −3.65 ‰. As for shallow and deep groundwater, mean $\delta^{18}O$ values were between −6.19 ‰ and −5.63 ‰. The isotopic composition of cave infiltration was also like the headwaters with a mean value of −5.80 ‰ (Table 1) but showed less variation as they were between −3.32 ‰ and −5.85 ‰ (Table 1). Mean *d*-excess values of headwaters and the Talgua river were between 15.04 ‰ and 16.70 ‰, whereas the mean *d*-excess values of shallow and groundwater were 12.21 ‰ and 13.87 ‰, respectively (Table 1). The mean *d*-excess value of cave infiltration was like the headwaters with mean values between 15.62 ‰. The overall variations in *d*-excess were also similar in the headwaters and cave infiltration (from 2.25 ‰ to 22.87 ‰), whereas in the Talgua river, *d*-excess varied from 8.59 ‰ to 23.52 ‰. Groundwater *d*-excess varied from 2.42 ‰ to 16.66 ‰. The LC-excess values followed similar

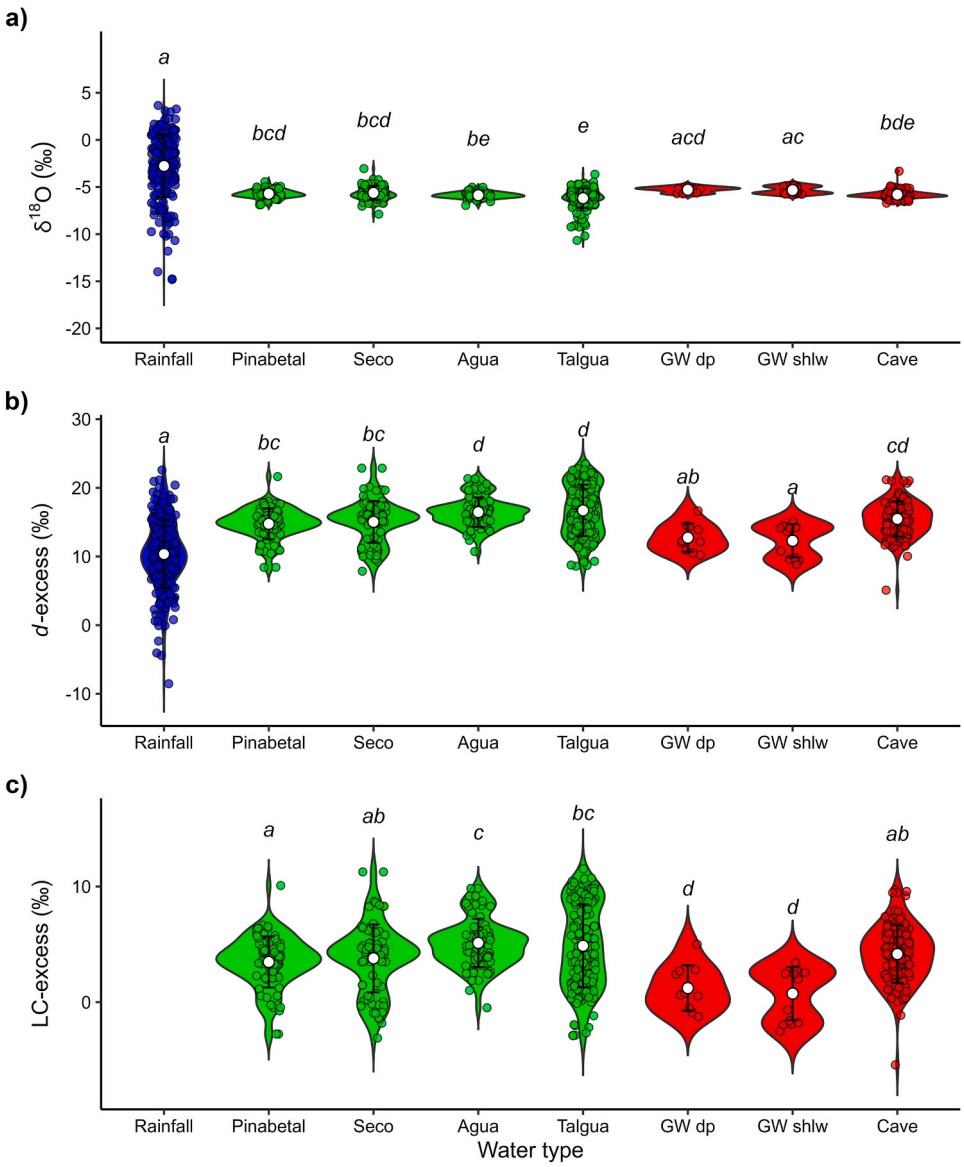

Fig. 5. Box plots of a) of $\delta^{18}O$ values (in ‰) for rainfall (N = 223), surface water (Pinabetal stream, N = 75; Seco stream, N = 79; Agua stream, N = 77, and Talgua river, N = 181), and groundwater (deep groundwater, N = 10; shallow groundwater, N = 14, and cave infiltration, N = 107). b) *d*-excess (in ‰) and c) LC-excess (in ‰) as described for panel a). Water types are color-coded (blue for rainfall, green for surface water, and red for groundwater), and plots include 25th, 75th, median, and outliers. We also report significance groupings where groups sharing at least one letter do not differ significantly at $p < 0.05$ based on Kruskal-Wallis non-parametric one-way analysis of variance on ranks. (For interpretation of the references to color in this figure legend, the reader is referred to the Web version of this article.)

variations as the *d*-excess (Table 1). Mean LC-excess values were higher in surface waters (headwaters and the Talgua river, 3.47 ‰–5.26 ‰) and cave infiltration, while shallow and deep groundwater showed lower means (0.74 ‰–1.21 ‰). Variability was also greater in surface waters and cave infiltration (−2.51 ‰–11.92 ‰) than in groundwater (−2.52 ‰–4.99 ‰). Rainfall had significantly higher $\delta^{18}O$ and lower *d*-excess compared to surface waters and groundwater ($p < 0.001$). Surface waters and cave infiltration had lower $\delta^{18}O$ but higher *d*-excess than shallow and deep groundwater ($p < 0.05$–0.001). Overall, LC-excess values were significantly greater in surface waters and cave infiltration than in groundwater across the Talgua River basin ($p < 0.01$).

3.4. The relationship between monthly rainfall and groundwater $\delta^{18}O$ ratios

A clear relationship between the monthly isotopic composition of rainfall and groundwater was identified with rainfall $^{18}O/^{16}O$ ratios > groundwater $^{18}O/^{16}O$ ratios (Fig. 6a). The mean P/GW ratio estimated for the Talgua River basin is 1.0020 ± 0.0027 (Fig. 6a). This value was calculated based on the amount-weighted rainfall isotope composition (average value: 3.58 ‰ or 1998 part per million in $^{18}O/^{16}O$) and the mean isotope composition of groundwater (i.e., shallow groundwater, deep groundwater, and cave infiltration, −5.53 ‰ or 1994 part per million in $^{18}O/^{16}O$). Despite the temporal variation of $\delta^{18}O$ ratios in groundwater shown in Fig. 3e, P/GW ratios are predominantly related to values > 1. As shown in Fig. 6b, variations in LC-excess values in groundwater with respect to groundwater $^{18}O/^{16}O$ ratios showed an indirect proportional relationship (i.e., lower LC-excess values were found in groundwater enriched in ^{18}O). However, this isotopic enrichment is not seasonally well-established, and it seems to be restricted to short-term variations in rainfall amounts, mostly during the dry season and after extended periods of reduced rainfall inputs (Fig. 3d and e).

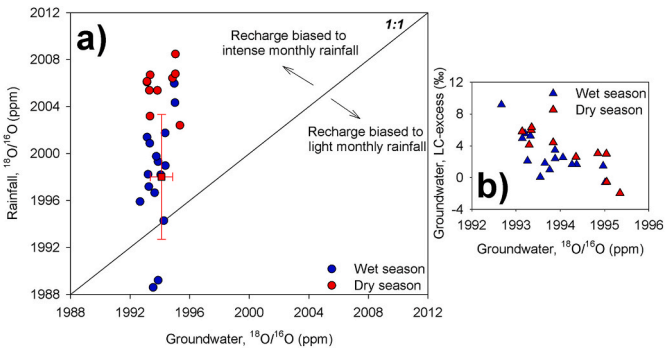

Fig. 6. Relationships between a) monthly rainfall and monthly groundwater $^{18}O/^{16}O$ ratios (in ppm, red circles for dry season, blue circles for wet season; modified from Jasechko and Taylor, 2015). The amount-weighted rainfall isotope composition and mean groundwater isotope composition are also shown (red square with error bars). B) The relationship between monthly LC-excess in groundwater and monthly groundwater $\delta^{18}O$ ratios as per dry and wet season (red and blue triangles, in that order) at Talgua River basin (September 2020–October 2022). (For interpretation of the references to color in this figure legend, the reader is referred to the Web version of this article.)

Based on the LC-excess values of cave infiltration and groundwater, we estimated the relative contributions of focused recharge (via preferential flow paths) and diffuse recharge to total recharge. During the dry season, focused recharge was the dominant source, contributing 99.6 ± 1.8 %, while diffuse recharge contributed only 0.4 ± 17.3 %. In the wet season, the contributions were more balanced, with focused recharge contributing 55.3 ± 36.9 % and diffuse recharge contributing 44.7 ± 29.8 %.

4. Discussion

4.1. Moisture sources and evolution assessment from surface water and groundwater isotopes

Our study period was mostly featured by La Niña and neutral conditions, with a strong La Niña developing between October 2021 and January 2023. Overall, colder waters in the Pacific Ocean allowed the intensification of easterlies (Caribbean Low-Level Jet, CLLJ) and an increase in the long-range moisture transport from the Caribbean basin to the isthmus (Durán-Quesada et al, 2017). This mechanism would naturally maximize the flux and convergence of Caribbean moisture onto the Caribbean slope of Honduras. The observation of 89 % Caribbean source contribution during our La Niña-dominated period likely represented a maximum or near-maximum state for the basin's moisture budget. In turn, El Niño is associated with the inverse impact on Central American hydroclimatology. It typically leads to drier-than-average conditions, due to a weaker CLLJ and increased vertical wind shear over the tropical North Atlantic, which suppresses convective activity and tropical cyclone formation (Amador, 2008; Sánchez-Murillo et al., 2016). Under these conditions, the relative contribution of other sources (11 %) like local evapotranspiration would see a relative increase, becoming a more significant component of the total precipitation budget.

The overall predominance of Caribbean air masses was related to inputs of trade-wind orographic rainfall, which were indicated by the isotopically enriched rainfall at the Talgua River basin with high $\delta^{18}O$ values (Guswa et al., 2007; Sánchez-Murillo et al., 2020). The estimated *d*-excess of ~10 ‰ for these rainfall events was also in agreement with the generation of rainfall at ocean's near-surface relative humidity (~85 %; Pfahl and Sodemann, 2014; Merlivat and Jouzel, 1979). The slope and intercept parameters of the LMWL of the Talgua River basin aligned with the GMWL (Craig, 1961, Fig. 3a) and it is like the LMWL estimated for the Caribbean slope of Central America (slope = 7.98, intercept = 9.49; Sánchez-Murillo et al., 2020).

Conversely, contributions of short-range air masses from the Gulf of Mexico, the Yucatan Peninsula, and the Pacific Ocean were mostly registered during the wet season. These rainfall inputs were characterized by lower $\delta^{18}O$ values and high *d*-excess. The significant difference between the *d*-excess of rainfall, surface water, and groundwater, suggested a substantial incorporation of recycled moisture (e.g., evapotranspiration fluxes). This significant water input has been also identified in mountainous areas of Costa Rica (Esquivel-Hernández et al., 2019; Guswa et al, 2007; Iraheta et al., 2021). The rainfall isotopic variability in the Talgua River basin corresponded with the influence of: i) significant rainfall generation due to the influence of cold fronts during the strongest period of NE trade winds (December–February) and ii) convective rainfall as result of a stronger activity of the ITCZ, eastern waves, and weaker NE trade winds during the wet season, which allowed the formation of rainfall events fed by evapotranspiration fluxes (García-Santos et al., 2021; Sánchez-Murillo and Birkel, 2016).

The propagation of the isotope composition of rainfall into the surface water and groundwater in the Talgua River basin confirmed complex interactions between moisture sources and hydrological processes in this karst region. Greater attenuation of the rainfall isotope composition in groundwater than in surface water may reflect complex water interactions with the karst system as water percolates downwards through the weathered carbonate bedrock immediately beneath the soil layer. Those zones are dominated by transmission rather than storage, delivering recharge to the saturated or phreatic zone (Li et al., 2024; Williams, 2008). The relationship between $\delta^{18}O$ and $\delta^{2}H$ showed a smaller slope and intercept in groundwater compared to surface waters, which may also be a result of complex hydrological interactions. This key difference initially suggests that groundwater recharge is controlled by matrix flow that is subject to evapoconcentration effects. In contrast, surface waters are part of a large porosity karstic system that allows rainfall to bypass extensive soil interaction.

Evaporation usually decreases the LC-excess during recharge in slow infiltration processes and significant low LC-excess values indicate strong evaporation effects (Landwehr and Coplen, 2006; Sprenger et al., 2017). However, temporal variations of $\delta^{18}O$ and LC-excess in groundwater in the karst system did not show significant evaporation effects in groundwater during water transit in the Talgua River basin. Thus, these temporal isotopic variations indicated that, depending on the capacity of the karst voids and the rainfall intensity, amounts of water rapidly flowed towards the phreatic zone via preferential flows (Jukić et al., 2021; Li et al., 2024). This fast recharge phenomenon was also evidenced by the strong variations of $\delta^{18}O$ in groundwater after drier periods, related to recharge from direct rainfall and faster water transit times with less mixing (Kirchner et al, 2010; Sánchez-Murillo et al., 2025). Therefore, despite the $\delta^{18}O$-$\delta^{2}H$ slope of groundwater suggesting minor evaporation occurred, the strong evidence from high LC-excess values shows that fast, focused recharge is the main mechanism water recharge the local groundwater system.

The variability of LC-excess may also be useful to identify karst water that interacted with recent precipitation, surface water, and then transferred to basin groundwater. It is also a proxy of the relationship between diffuse recharge from soil water in the connected porosity and focused recharge directly from precipitation via preferential paths (Clark and Fritz, 1997; Hartmann et al., 2014; Hao et al., 2023). The overall similarity between the LC-excess of surface water at different elevations and the LC-excess of cave infiltration (~4 ‰, Fig. 5c) also confirmed major contributions from focused recharge via preferential flow paths which are modulated by the rainfall variability. Even though LC-excess values in groundwater were lower than in surface water and cave infiltration, the overall difference is relatively small which additionally suggested that recharge occurred by rapid infiltration with little evaporation prior to recharge and fast water transit times. Such high infiltration rates were also observed in karst systems because surface water quickly enters the subsurface through sinkholes, fractures, and

conduits in the underlying bedrock. (Ding et al., 2020; Guo et al., 2018; Li et al., 2024).

4.2. Isotope-inferred groundwater recharge mechanisms

The comparison of the isotopic composition of groundwater and rainfall can be applied to estimate recharge in tropical karst aquifers and to assess recharge mechanisms with respect to the seasonal distribution of rainfall (Jasechko and Taylor, 2015; Jones and Banner, 2003). In the Talgua River basin, isotopic variations in rainfall (e.g., $\delta^{18}O$ and *d*-excess) were well transferred to the catchment karst water (i.e., cave infiltration) and groundwater which suggest major contributions of focused recharge via rapid conduit flows. The single-isotope mass balance, calculated based on LC-excess values, confirmed this predominance. This finding suggests that under non-saturated conditions (i.e., when more conductive karst structures like intermediate conduits and voids are mostly empty), rainfall inputs are rapidly transferred to the local aquifer system. In turn, under wet season conditions, the system gets closer to diffuse conditions indicating a more balanced contribution of the advection flow process (McGuire et al., 2002; Salas-Navarro et al., 2018). Recharge was also seasonally biased to the more intense rainy period. This was clearly indicated by: i) the systematic P/GW $^{18}O/^{16}O$ ratios >1 during ~2 year period (i.e., higher $\delta^{18}O$ in rainfall than in groundwater, Fig. 6a) and ii) high *d*-excess in surface water and groundwater due to the substantial incorporation of recycled moisture via convective rainfall during the stronger activity of the ITCZ and eastern waves in the wet season. Jasechko and Taylor (2015) estimated a precipitation threshold intensity decile (>80th) of ~170 mm/month for significant groundwater recharge at the limestone aquifers of Barbados and of ~310 mm/month (>70th decile) at the limestone aquifer of Guam. Based on the long-term precipitation records available for Catacamas (Fig. 2), average monthly rainfall from May to November is 155 mm/month with a maximum value of 215 mm/month. These monthly rainfall amounts are like the rainfall threshold estimated for these island tropical karst aquifers and like other recent global-scale estimations of diffuse groundwater recharge in karst areas (Jones and Banner, 2003; Wan et al., 2024). However, the overall distribution of P/GW ratios, relative to the amount-weighted mean and its uncertainty (1.0020 ± 0.0027), indicates that during the dry season or drier-than-normal periods (e.g., MSD), local recharge can still incorporate water inputs from rainfall events with intensities smaller than those registered during the wet season. This also suggests the contribution of enriched orographic rainfall from the Caribbean Sea to the local recharge.

The isotopic composition of groundwater can also serve as a proxy of cumulative recharge to the aquifer systems. As for the Talgua River basin, the high variability of $\delta^{18}O$ in groundwater in comparison to surface water may indicate that recharge rates may be spatially homogeneous across the catchment and higher rates are not necessarily found at higher elevations. Recharge from surface water systems like Talgua river may be also possible. The monthly variation of LC-excess with respect to $^{18}O/^{16}O$ ratios in groundwater (Fig. 6b) also showed no seasonality and indicated low evaporation conditions, also reflecting spatial homogenous and rapid recharge rates. In other karst systems, where much larger and thicker karst structures can be found (e.g., Puerto Rico and Slovenia), much longer groundwater flow paths and residence times are reported. As for the Talgua River basin, the karst system seems to display shorter flow components and more direct contact with the underlying aquifer (Jones and Banner, 2003; Rusjan et al., 2019). However, further investigations may serve to identify the presence of more complex karst in the Talgua River basin like dual-porosity structures, where during heavier rainfall events, the more conductive karst structure controlled the system response, and the weathered porosity structure of the epikarst and vadose zone controlled the hydrogeological response during drier periods (Hepach et al., 2024; Jódar et al., 2025).

The assessment of recharge response in karst aquifers to rainfall gradients may help to predict how these systems will respond to changing climatic conditions and can inform adaptation strategies (Dunkerley, 2020; Shen et al., 2022). Overall, variations in rainfall event types have shown pronounced differences in runoff coefficients indicating contrasting levels of hydrologic connectivity (Saavedra et al., 2022). Sánchez-Murillo et al. (2025) identified the rapid propagation of extreme rainfall events (i.e., tropical cyclones) and their isotopic composition as clear isotope excursions in surface water and groundwater in the Talgua River basin. During the influence of Hurricane Eta, Iota, and Bonnie in 2020 and 2022, respectively, a significant increase in the P/SW and P/GW $\delta^{18}O$ ratios (with values up to ~3) was evident in the Talgua River basin, reflecting the dominant contribution of strong convective rainfall, a clear deviation from baseflow isotope compositions, and significantly different than the amount-weighted mean P/GW estimated this study.

4.3. Implications for future water resources management in the Talgua River basin

Our findings are relevant to establishing management strategies to protect water quality in the Talgua River basin given the ongoing land-use changes, such as deforestation and tillage, which can increase soil erosion over the karst environment. We consider these new insights particularly useful for areas in the mid-to-lower section of the Talgua River basin, where vegetation cover has been cleared for cattle ranching and subsistence farming (Reyes-Sandoval and Serrano-Rodríguez, 2021). In these specific areas, the overall share of forest cover (72 %) to pastureland and crops (21 %) is likely different from these average values because of increasing land transformation for agricultural use. The transformation of forests into croplands and pastures in the Talgua River basin may fundamentally change the basin's hydrological cycle by changing how water partitioned and infiltrated. The primary effect is a significant reduction in evapotranspiration, as the shallow roots of crops and pastureland cannot match the high-water uptake and interception of deep-rooted forest trees (Jasechko et al., 2014; Kirchner et al., 2020). Thus, it is essential that local authorities protect the upper part of the basin, where soils are still covered by broadleaf forest, and prevent the expansion of agricultural frontier areas that have been cleared to establish crops like coffee farms.

Removing forest covers may also accelerate soil compaction from agriculture, which subsequently could cause an increase in surface runoff and a reduction in the soil's capacity for diffuse infiltration (Peng and Wang, 2011; Toohey et al., 2017). Depending on the intensity of rainfall and the saturation excess runoff phase in the karst permeable structures, faster runoff and concentrated input to the karst conduit network may cause a rapid hydrological response, resulting in higher peak flows and an increased risk of flash flooding at springs and surface outlets following rainfall. Other studies have reported that land use changes lead to alterations in groundwater recharge, subsequently causing a reduction of the flow discharge in the local springs, and a decrease in baseflow (dry season flow), making water availability less stable during dry periods (Bittner et al., 2018; Guo et al., 2018; Smith et al., 2020). Diverse land-use gradients (e.g., agriculture, urban development, natural forests) may also alter flow patterns and impact on the water quality due to the introduction of a variety of potential contaminants into the groundwater system. Increasing rapid and focused recharge of karst aquifers, which naturally lack filtration, means that water quality is severely degraded due to the transport of high loads of sediment, nutrients, and agrochemicals directly into the groundwater system, greatly increasing the risk of contamination (Moreno-Gómez et al., 2023; Reberski et al., 2021).

In karst aquifer systems, adaptation strategies may focus on the implementation of managed aquifer recharge (MAR) techniques and a more robust water quality protection (Levintal et al., 2022). However, implementation of MAR techniques needs to consider many aspects (e.g., heterogeneities in surface and/or subsurface characteristics, variable groundwater qualities, recharge method, water recovery) which make

the issues of site selection for MAR challenging (Zhang et al, 2020). Thus, for karst systems in developing countries like Honduras, effective and simple strategies, focusing on vulnerability reduction and event-based management, are potentially better implemented. To reduce the negative effects of ongoing land use changes in the Talgua River basin, priority protection zones must be established immediately around high-vulnerability features like sinkholes and losing streams, strictly regulating land use, pollution sources, and infrastructure development within these areas (Luo et al., 2019; Kidmose et al., 2023). Moreover, effective protection may need a robust extreme event monitoring protocol, involving targeted and rapid-response monitoring of physical variables like turbidity (i.e., a strong proxy for particulate contaminants and pathogen transport, Fernández-Ortega et al., 2023) during and immediately following high-intensity rainfall, allowing for timely and adaptive measures such as issuing public health advisories. Furthermore, protecting the aquifer requires implementing better land-use practices in recharge areas to reduce contaminant loads from agriculture and strengthening wastewater treatment to safeguard the water quality during the fast transport times characteristic of karst systems (Jain, 2023; Levintal et al., 2022)

5. Conclusions

Our study provided essential insights into the hydrological processes of the Talgua River basin, northeastern Honduras, revealing complex interactions of moisture transport, rainfall generation, and the surface-groundwater systems as well as the dynamic nature of water transport and mixing within this tropical karst environment. The isotopic analysis of rainfall in the Talgua River basin revealed a hydrological system primarily influenced by Caribbean moisture, leading to isotopically heavy rainfall (i.e., high $\delta^{18}O$ values) via trade-wind orographic rainfall and depleted excursions (i.e., low $\delta^{18}O$ values) but significant inputs of recycled moisture from continental ET during the wet season. This complex rainfall isotopic signal rapidly propagated into the karst system's surface water and groundwater, suggesting that focused recharge via preferential flow paths (like conduits and fractures) is the dominant mechanism, particularly during the intense rainy season. While soil-water interactions cause a degree of isotopic attenuation and evaporation effects in the groundwater, the overall small differences between water sources confirm rapid infiltration and short water transit times, consistent with a highly conductive, albeit potentially complex (e.g., dual-porosity), tropical karst aquifer. It is worth noting that our results may be improved by expanding the rainfall sampling network to include more stations strategically placed across the altitudinal gradient in the Talgua River basin, ensuring continuous isotopic data collection. Improvement may also be achieved by collecting groundwater samples at different elevations and discrete depths (e.g., shallow epikarst, intermediate conduits, and deep phreatic zones) within the karst-dominated areas. Moreover, HYSPLIT backward trajectories analysis should be applied comparatively to both ENSO warm phases (El Niño) and cold phases (La Niña) to better identify moisture source regions and transport mechanisms. Future studies may also implement other environmental tracers (e.g., hydrochemistry, fluorescent dyes) and age dating techniques (e.g., tritium, CFCs) alongside a depth-specific groundwater sampling network.

This comprehensive isotopic assessment not only improved our knowledge of groundwater recharge characteristics in tropical karst regions but also provided useful baseline information for future research. These insights can be essential for developing effective water management and protection strategies in the Talgua River basin, especially given the recent changes in land use (including the conversion of primary forests to coffee plantations and degraded pastures) which require urgent attention as they may limit the basin's capacity for water production due to the key role water vapor recycling plays in generating rainfall in the Talgua River basin. Moreover, our findings underline a critical challenge in tropical karst environments like the Talgua River basin: while rainfall is essential, intense rain events contribute less effectively to the long-term recharge of groundwater systems. This rapid flow may have severe negative impact on water quality and accelerate soil erosion. This process may also facilitate the immediate transport of surface contaminants into groundwater sources, thus increasing the risk of both flash flooding and sporadic water quality crises.

CRediT authorship contribution statement

Jorge Cardona-Hernández: Writing – original draft, Project administration, Formal analysis, Data curation, Conceptualization. **Germain Esquivel-Hernández:** Writing – original draft, Supervision, Project administration, Methodology, Funding acquisition, Formal analysis, Data curation, Conceptualization. **Lucilena Rebelo Monteiro:** Writing – review & editing, Methodology, Formal analysis, Data curation. **Ricardo Sánchez-Murillo:** Writing – review & editing, Methodology, Investigation, Formal analysis. **Marycel E.B. Cotrim:** Writing – review & editing, Methodology, Data curation. **Rolando Sánchez-Gutiérrez:** Writing – review & editing. **Christian Birkel:** Writing – review & editing. **Tania Peña-Paz:** Writing – review & editing. **Laura Benegas-Negri:** Writing – review & editing.

Declaration of competing interest

The authors declare that they have no known competing financial interests or personal relationships that could have appeared to influence the work reported in this paper.

Acknowledgements

The authors thank the Research and Graduate Studies Department at Universidad Nacional de Agricultura of Honduras (UNAG) for its financial support for this research. We thank the Honduran Institute of Earth Sciences at Universidad Nacional de Autónoma of Honduras (UNAH) for its valuable contribution in promoting the national isotope monitoring network in Honduras. We thank the National Center for Oceanographic, Atmospheric, and Seismic Studies (CENAOS) and the Permanent Contingency Committee (COPECO) for their support in providing the meteorological information used in this research. The authors thank the Stable Isotopes Research Group at Universidad Nacional Costa Rica for providing the access to water stable isotope analysis for this study. DOCINADE. The authors gratefully acknowledge the NOAA Air Resources Laboratory (ARL) for the provision of the HYSPLIT transport and dispersion model and/or READY website (https://www.ready.noaa.gov) used in this publication.

Data statement

The datasets presented in this study are accessible at Mendeley Data, https://data.mendeley.com/datasets/wkxpjxxs74/1 (Cardona-Hernandez et al., 2025).

References

Amador, J., 2008. The intra-Americas seas low-level jet (IALLJ): overview and future research. Ann. N. Y. Acad. Sci. 1146, 153–188. https://doi.org/10.1196/annals.1446.012.

Arbel, Y., Greenbaum, N., Lange, J., Inbar, M., 2010. Infiltration processes and flow rates in developed karst vadose zone using tracers in cave drips. Earth Surf. Process. Landf. 35 (14), 1682–1693. https://doi.org/10.1002/esp.2010.

Bakalowicz, M., 2005. Karst groundwater: a challenge for new resources. Hydrogeol. J. 13 (1), 148–160. https://doi.org/10.1007/s10040-004-0402-9.

Berg, P., Moseley, C., Haerter, J.O., 2013. Strong increase in convective precipitation in response to higher temperatures. Nat. Geosci. 6 (3), 181–185. https://doi.org/10.1038/ngeo1731.

Bittner, D., Narany, T.S., Kohl, B., Disse, M., Chiogna, G., 2018. Modeling the hydrological impact of land use change in a dolomite-dominated karst system. J. Hydrol. 567, 267–279. https://doi.org/10.1016/j.jhydrol.2018.10.017.

Bresinsky, L., Kordilla, J., Hector, T., Engelhardt, I., Livshitz, Y., Sauter, M., 2023. Managing climate change impacts on the Western Mountain Aquifer: implications for Mediterranean karst groundwater resources. J. Hydrol. X 20, 100153. https://doi.org/10.1016/j.hydroa.2023.100153.

Camin, F., Besic, D., Brewer, P.J., Allison, C.E., Coplen, T.B., Dunn, P.J.H., Gehre, M., Gröning, M., Meijer, H.a.J., Hélie, J., Iacumin, P., Kraft, R., Krajnc, B., Kümmel, S., Lee, S., Meija, J., Mester, Z., Mohn, J., Moossen, H., Wielgosz, R.I., 2025. Stable isotope reference materials and Scale Definitions—Outcomes of the 2024 IAEA experts meeting. Rapid Commun. Mass Spectrom. 39 (14). https://doi.org/10.1002/rcm.10018.

Cardona-Hernandez, J., Esquivel-Hernandez, G., Monteiro, L., Sanchez-Murillo, R., Cotrim, M.E.B., Sanchez-Gutierrez, R., Birkel, C., Peña-Paz, T., Benegas-Negri, L., 2025. First isotopic study of the Talgua River Basin, Honduras. Mendeley Data, V1. https://doi.org/10.17632/wkxpjxxs74.1.

Clark, I.D., Fritz, P., 1997. Environmental Isotopes in Hydrogeology. Lewis, Boca Raton, Florida.

Craig, H., 1961. Isotopic variations in meteoric waters. Science 133 (3465), 1702–1703. https://doi.org/10.1126/science.133.3465.1702.

Dansgaard, W., 1964. Stable isotopes in precipitation. Tellus 16 (4), 436–468. https://doi.org/10.3402/tellusa.v16i4.8993.

Ding, H., Zhang, X., Chu, X., Wu, Q., 2020. Simulation of groundwater dynamic response to hydrological factors in karst aquifer system. J. Hydrol. 587, 124995. https://doi.org/10.1016/j.jhydrol.2020.124995.

Dixon, B., Hasemann, G., Gomez, P., Brady, J., Beaudry-Corbett, M., 1998. Multiethnicity or multiple enigma: archaeological survey and cave exploration in the Río Talgua drainage. Honduras. Ancient Mesoamerica 9, 327–340.

Dunkerley, D., 2020. Rainfall intensity in geomorphology: challenges and opportunities. Prog. Phys. Geogr. Earth Environ. 45 (4), 488–513. https://doi.org/10.1177/0309133320967893.

Dunn, O.J., 1961. Multiple comparisons among means. J. Am. Stat. Assoc. 56 (293), 52–64. https://doi.org/10.1080/01621459.1961.10482090.

Durán-Quesada, A.M., Gimeno, L., Amador, J., 2017. Role of moisture transport for Central American precipitation. Earth Syst. Dyn. 8 (1), 147–161. https://doi.org/10.5194/esd-8-147-2017.

Emanuel, K., 2021. Atlantic tropical cyclones downscaled from climate reanalyses show increasing activity over past 150 years. Nat. Commun. 12 (1). https://doi.org/10.1038/s41467-021-27364-8.

Ensley, R., Hansen, R.D., Morales-Aguilar, C., Thompson, J., 2021. Geomorphology of the Mirador-Calakmul Karst Basin: a GIS-based approach to hydrogeologic mapping. PLoS One 16 (8), e0255496. https://doi.org/10.1371/journal.pone.0255496.

Esquivel-Hernández, G., Mosquera, G.M., Sánchez-Murillo, R., Quesada-Román, A., Birkel, C., Crespo, P., Célleri, R., Windhorst, D., Breuer, L., Boll, J., 2019. Moisture transport and seasonal variations in the stable isotopic composition of rainfall in Central American and Andean Páramo during El Niño conditions (2015–2016). Hydrol. Process. 33 (13), 1802–1817. https://doi.org/10.1002/hyp.13438.

Fernández-Ortega, J., Barberá, J.A., Andreo, B., 2023. Real-time karst groundwater monitoring and bacterial analysis as early warning strategies for drinking water supply contamination. Sci. Total Environ. 912, 169539. https://doi.org/10.1016/j.scitotenv.2023.169539.

Finch, R., Pistole, N., 2011. Honduras: Caving in Conglomerate. Digital Commons@ University of South Florida. https://digitalcommons.usf.edu/kip_articles/2560.

Fleming, Z.L., Monks, P.S., Manning, A.J., 2012. Review: untangling the influence of air-mass history in interpreting observed atmospheric composition. Atmos. Res. 104–105, 1–39. https://doi.org/10.1016/j.atmosres.2011.09.009.

Ford, D., Williams, P., 2007. Karst Hydrogeology and Geomorphology. John Wiley and Sons Ltd, West Sussex, England. https://doi.org/10.1002/9781118684986.

Fowler, H.J., Lenderink, G., Prein, A.F., Westra, S., Allan, R.P., Ban, N., Barbero, R., Berg, P., Blenkinsop, S., X, H.D.O., Guerreiro, S., Haerter, J.O., Kendon, E.J., Lewis, E., Schaer, C., Sharma, A., Villarini, G., Wasko, C., Zhang, X., 2021. Anthropogenic intensification of short-duration rainfall extremes. Nat. Rev. Earth Environ. 2 (2), 107–122. https://doi.org/10.1038/s43017-020-00128-6.

Froehlich, K., Gibson, J.J., Aggarwal, P., 2001. Deuterium excess in precipitation and its climatological significance. In: Study of Environmental Change Using Isotope Techniques. Proceedings International Conference Vienna, pp. 54–66. Austria.

García-Santos, S., Sánchez-Murillo, R., Peña-Paz, T., Chirinos-Escobar, M., Hernández-Ortiz, J., Mejía-Escobar, E.J., Ortega, L., 2021. Water stable isotopes reveal groundwater vulnerability to land use fragmentation and climate variability in central Honduras. SSRN Electron. J. https://doi.org/10.2139/ssrn.3994615.

Giese, M., Caballero, Y., Hartmann, A., Charlier, J., 2025. Trends in long-term hydrological data from European karst areas: insights for groundwater recharge evaluation. Hydrol. Earth Syst. Sci. 29 (14), 3037–3054. https://doi.org/10.5194/hess-29-3037-2025.

Giorgi, F., 2006. Climate change hot-spots. Geophys. Res. Lett. 33, 8. https://doi.org/10.1029/2006GL025734.

Good, S.P., Noone, D., Bowen, G., 2015. Hydrologic connectivity constrains partitioning of global terrestrial water fluxes. Science 349 (6244), 175–177. https://doi.org/10.1126/science.aaa5931.

Gröning, M., Lutz, H., Roller-Lutz, Z., Kralik, M., Gourcy, L., Pöltenstein, L., 2012. A simple rain collector preventing water re-evaporation dedicated for δ18O and δ2H analysis of cumulative precipitation samples. J. Hydrol. 448–449, 195–200. https://doi.org/10.1016/j.jhydrol.2012.04.041.

Guo, Y., Wu, Q., Jiang, G., Han, Z., Tang, Q., Quan, X., 2018. Dynamic variation characteristics of water chemistries and isotopes in a typical karst aquiferous system and their implications for the local karst water cycle, Southwest China. Carbonates Evaporites 34 (3), 987–1001. https://doi.org/10.1007/s13146-018-0457-7.

Guswa, A.J., Rhodes, A.L., Newell, S.E., 2007. Importance of orographic precipitation to the water resources of Monteverde, Costa Rica. Adv. Water Resour. 30 (10), 2098–2112. https://doi.org/10.1016/j.advwatres.2006.07.008.

Hanson, D.L., Steenhuis, T.S., Walter, M.F., Boll, J., 2004. Effects of soil degradation and management practices on the surface water dynamics in the Talgua River Watershed in Honduras. Land Degrad. Dev. 15 (4), 367–381. https://doi.org/10.1002/ldr.603.

Hao, Z., Gao, Y., Zhang, Q., Wen, W., 2023. Isotopic insights on quantitative assessments of interaction of eco-hydrological processes in multi-scale karst watersheds. Int. Soil Water Conserv. Res. 12 (1), 156–170. https://doi.org/10.1016/j.iswcr.2023.05.001.

Hartmann, A., Goldscheider, N., Wagener, T., Lange, J., Weiler, M., 2014. Karst water resources in a changing world: review of hydrological modeling approaches. Rev. Geophys. 52 (3), 218–242. https://doi.org/10.1002/2013rg000443.

Hepach, P., Bresinsky, L., Sauter, M., Livshitz, Y., Engelhardt, I., 2024. Comparaison de méthodes de calcul de la recharge des eaux souterraines pour des aquifères karstiques sous climat méditerranéen. Hydrogeol. J. 32 (5), 1377–1396. https://doi.org/10.1007/s10040-024-02809-8.

Hughes, C.E., Crawford, J., 2012. A new precipitation weighted method for determining the meteoric water line for hydrological applications demonstrated using Australian and global GNIP data. J. Hydrol. 464–465, 344–351. https://doi.org/10.1016/j.jhydrol.2012.07.029.

Iraheta, A., Birkel, C., Benegas, L., Ríos, N., Sánchez-Murillo, R., Beyer, M., 2021. A preliminary isotope-based evapotranspiration partitioning approach for tropical Costa Rica. Ecohydrology 14 (5). https://doi.org/10.1002/eco.2297.

Jain, H., 2023. Groundwater vulnerability and risk mitigation: a comprehensive review of the techniques and applications. Groundw. Sustain. Dev. 22, 100968. https://doi.org/10.1016/j.gsd.2023.100968.

Jasechko, S., Taylor, R.G., 2015. Intensive rainfall recharges tropical groundwaters. Environ. Res. Lett. 10 (12), 124015. https://doi.org/10.1088/1748-9326/10/12/124015.

Jasechko, S., Birks, S.J., Gleeson, T., Wada, Y., Fawcett, P.J., Sharp, Z.D., McDonnell, J. J., Welker, J.M., 2014. The pronounced seasonality of global groundwater recharge. Water Resour. Res. 50 (11), 8845–8867. https://doi.org/10.1002/2014wr015809.

Jeannin, P., Artigue, G., Butscher, C., Chang, Y., Charlier, J., Duran, L., Gill, L., Hartmann, A., Johannet, A., Jourde, H., Kavousi, A., Liesch, T., Liu, Y., Lüthi, M., Malard, A., Jódar, J., Morales-González, A.L., Urrutia, J., Herrera, C., Lambán, L.J., Martos-Rosillo, S., González-Ramón, A., 2025. Characterisation of mountain-Mediterranean karst aquifers as lighthouses for the assessment of global change impacts in the Mediterranean region: the Sierra Seca aquifer system (SE Spain). Sci. Total Environ. 985, 179719. https://doi.org/10.1016/j.scitotenv.2025.179719.

Jódar, J., Morales-González, A.L., Urrutia, J., Herrera, C., Lambán, L.J., Martos-Rosillo, S., González-Ramón, A., 2025. Characterisation of mountain-Mediterranean karst aquifers as lighthouses for the assessment of global change impacts in the Mediterranean region: the Sierra Seca aquifer system (SE Spain). Sci. Total Environ. 985, 179719. https://doi.org/10.1016/j.scitotenv.2025.179719.

Jones, I.C., Banner, J.L., 2003. Estimating recharge thresholds in tropical karst island aquifers: barbados, Puerto Rico and Guam. J. Hydrol. 278 (1–4), 131–143. https://doi.org/10.1016/s0022-1694(03)00138-0.

Jukić, D., Denić-Jukić, V., Lozić, A., 2021. An alternative method for groundwater recharge estimation in karst. J. Hydrol. 600, 126671. https://doi.org/10.1016/j.jhydrol.2021.126671.

Kidmose, J., Nilsson, B., Klem, N.K., Pedersen, P.G., Henriksen, H.J., Sonnenborg, T.O., 2023. Can effective porosity be used to estimate near-well protection zones in fractured chalk? Hydrogeol. J. 31 (8), 2197–2212. https://doi.org/10.1007/s10040-023-02743-1.

Kirchner, J.W., Tetzlaff, D., Soulsby, C., 2010. Comparing chloride and water isotopes as hydrological tracers in two Scottish catchments. Hydrol. Process. 24 (12), 1631–1645. https://doi.org/10.1002/hyp.7676.

Kirchner, J.W., Berghuijs, W.R., Allen, S.T., Hrachowitz, M., Hut, R., Rizzo, D.M., 2020. Streamflow response to forest management. Nature 578 (7794), E12–E15. https://doi.org/10.1038/s41586-020-1940-6.

Kottek, M., Grieser, J., Beck, C., Rudolf, B., Rubel, F., 2006. World Map of the Köppen-Geiger climate classification updated. Meteorol. Z. 15 (3), 259–263. https://doi.org/10.1127/0941-2948/2006/0130.

Kruskal, W.H., Wallis, W.A., 1952. Use of ranks in One-Criterion variance analysis. J. Am. Stat. Assoc. 47 (260), 583–621. https://doi.org/10.1080/01621459.1952.10483441.

Landwehr, J.M., Coplen, T.B., 2006. Line-conditioned excess: a new method for characterizing stable hydrogen and oxygen isotope ratios in hydrologic systems. Paper Presented at International Conference on Isotopes in Environmental Studies. International Atomic Energy Agency, Vienna, pp. 132–135.

Levintal, E., Kniffin, M.L., Ganot, Y., Marwaha, N., Murphy, N.P., Dahlke, H.E., 2022. Agricultural managed aquifer recharge (Ag-MAR)—A method for sustainable groundwater management: a review. Crit. Rev. Environ. Sci. Technol. 53 (3), 291–314. https://doi.org/10.1080/10643389.2022.2050160.

Li, Z., Chen, X., Liu, W., Si, B., 2017. Determination of groundwater recharge mechanism in the deep loessial unsaturated zone by environmental tracers. Sci. Total Environ. 586, 827–835. https://doi.org/10.1016/j.scitotenv.2017.02.061.

Li, H., Xiang, W., Si, B., Min, M., Miao, C., Jin, J., 2024. Quantifying recharge mechanisms in low-hilly areas of a loess region: implications for the quantity and quality of groundwater. J. Hydrol., 131982 https://doi.org/10.1016/j.jhydrol.2024.131982.

Liu, H., Tang, J., Chen, L., Zhang, X., Zhu, B., Liang, C., Liu, C., Wang, G., 2022. Threshold recognition for shallow groundwater recharge by precipitation using dual isotopes in a small subtropical hilly catchment. Catena 213, 106186. https://doi.org/10.1016/j.catena.2022.106186.

Luo, Q., Yang, Y., Qian, J., Wang, X., Chang, X., Ma, L., Li, F., Wu, J., 2019. Spring protection and sustainable management of groundwater resources in a spring field. J. Hydrol. 582, 124498. https://doi.org/10.1016/j.jhydrol.2019.124498.

McGuire, K., DeWalle, Gburek, W., 2002. Evaluation of mean residence time in subsurface waters using oxygen-18 fluctuations during drought conditions in the mid-Appalachians. J. Hydrol. 261 (1–4), 132–149. https://doi.org/10.1016/s0022-1694(02)00006-9.

Merlivat, L., Jouzel, J., 1979. Global climate interpretation of the deuterium-oxygen 18 relationship for precipitation. J. Geophys. Res. 84 (C8), 5029–5033. https://doi.org/10.1029/JC084iC08p0502.

Michelle-Warner, M., 2016. A Biogeochemistry Approach to Geographic Origin and Mortuary Arrangement at the Talgua Cave Ossuaries, Olancho, Honduras. Master of Arts Thesis. Mississippi State University, USA.

Moreno-Gómez, M., Liedl, R., Stefan, C., Pacheco, J., 2023. Theoretical analysis and considerations of the main parameters used to evaluate intrinsic karst groundwater vulnerability to surface pollution. Sci. Total Environ. 907, 167947. https://doi.org/10.1016/j.scitotenv.2023.167947.

Ochoa-Alvarez, R., Mckittrick, R., Raudales, R., Flores-Molina, M., Gonzales, L., 1989. Hydrogeological Map of the Republic of Honduras. Instituto Geográfico Nacional and Servicio Autonomo Nacional de Acueductos y Alcantarillados, Honduras (in Spanish).

Peng, T., Wang, S., 2011. Effects of land use, land cover and rainfall regimes on the surface runoff and soil loss on karst slopes in southwest China. Catena 90, 53–62. https://doi.org/10.1016/j.catena.2011.11.001.

Pfahl, S., Sodemann, H., 2014. What controls deuterium excess in global precipitation? Clim. Past 10 (2), 771–781. https://doi.org/10.5194/cp-10-771-2014.

Reberski, J.L., Terzić, J., Maurice, L.D., Lapworth, D.J., 2021. Emerging organic contaminants in karst groundwater: a global level assessment. J. Hydrol. 604, 127242. https://doi.org/10.1016/j.jhydrol.2021.127242.

Reyes-Sandoval, J.T., Serrano-Rodríguez, A., 2021. Análisis morfométrico y biofísico en la cuenca del Río Talgua, Honduras. Ciencia Latina Revista Científica Multidisciplinar 5 (6), 12024–12042. https://doi.org/10.37811/cl_rcm.v5i6.1214.

Rusjan, S., Sapač, K., Petrič, M., Lojen, S., Bezak, N., 2019. Identifying the hydrological behavior of a complex karst system using stable isotopes. J. Hydrol. 577, 123956. https://doi.org/10.1016/j.jhydrol.2019.123956.

Saavedra, F.A., Musolff, A., Von Freyberg, J., Merz, R., Basso, S., Tarasova, L., 2022. Disentangling scatter in long-term concentration–discharge relationships: the role of event types. Hydrol. Earth Syst. Sci. 26 (23), 6227–6245. https://doi.org/10.5194/hess-26-6227-2022.

Sadeghi, B., 2025. Clustering in geo-data science: navigating uncertainty to select the most reliable method. Ore Geol. Rev., 106591 https://doi.org/10.1016/j.oregeorev.2025.106591.

Salas-Navarro, J., Sánchez-Murillo, R., Esquivel-Hernández, G., Corrales-Salazar, J.L., 2018. Hydrogeological responses in tropical mountainous springs. Isot. Environ. Health Stud. 55 (1), 25–40. https://doi.org/10.1080/10256016.2018.1546701.

Sánchez-Murillo, R., Durán-Quesada, A.M., Esquivel-Hernández, G., Rojas-Cantillano, D., Birkel, C., Welsh, K., Sánchez-Llull, M., Alonso-Hernández, C.M., Tetzlaff, D., Soulsby, C., Boll, J., Kurita, N., Cobb, K.M., 2019. Deciphering key processes controlling rainfall isotopic variability during extreme tropical cyclones. Nat. Commun. 10 (1). https://doi.org/10.1038/s41467-019-12062-3.

Sánchez-Murillo, R., Birkel, C., 2016. Groundwater recharge mechanisms inferred from isoscapes in a complex tropical mountainous region. Geophys. Res. Lett. 43 (10), 5060–5069. https://doi.org/10.1002/2016gl068888.

Sánchez-Murillo, R., Durán-Quesada, A.M., Birkel, C., Esquivel-Hernández, G., Boll, J., 2016. Tropical precipitation anomalies and d-excess evolution during El Niño 2014-16. Hydrol. Process. https://doi.org/10.1002/hyp.11088, 2016.

Sánchez-Murillo, R., Esquivel-Hernández, G., Corrales-Salazar, J.L., Castro-Chacón, L., Durán-Quesada, A.M., Guerrero-Hernández, M., Delgado, V., Barberena, J., Montenegro-Rayo, K., Calderón, H., Chevez, C., Peña-Paz, T., García-Santos, S., Ortiz-Roque, P., Alvarado-Callejas, Y., Benegas, L., Hernández-Antonio, A., Matamoros-Ortega, M., Ortega, L., Terzer-Wassmuth, S., 2020. Tracer hydrology of the data-scarce and heterogeneous Central American Isthmus. Hydrol. Process. https://doi.org/10.1002/hyp.13758.

Sánchez-Murillo, R., Herrera, D.A., Farrick, K.K., Esquivel-Hernández, G., Sánchez-Gutiérrez, R., Barberena-Moncada, J., Guatemala-Herrera, J., Flores-Meza, Y., Cerón-Pineda, R., Gil-Urrutia, L., Cardona-Hernández, J., Peña-Paz, T., Hernández-Ortiz, J.O., Harrison-Smith, W., Marshall, G., Persoiu, A., Pérez-Quezadas, J., Mejía-González, M., González-Hita, L., Dee, S.G., 2025. Stable isotope tempestology of tropical cyclones across the North Atlantic and Eastern Pacific Ocean basins. Ann. N. Y. Acad. Sci. https://doi.org/10.1111/nyas.15274.

Saravia-Maldonado, S.A., Fernández-Pozo, L.F., Ramírez-Rosario, B., Rodríguez-González, M.Á., 2024. Analysis of deforestation and water quality in the Talgua River Watershed (Honduras): ecosystem approach based on the DPSIR model. Sustainability 16 (12), 5034. https://doi.org/10.3390/su16125034.

Shen, H., Xu, Y., Liang, Y., Zhao, C., Wang, Z., Zhang, Z., Qi, J., 2022. Review: groundwater recharge estimation in southern China karst regions. Carbonates Evaporites 38 (1). https://doi.org/10.1007/s13146-022-00841-x.

Skrzypek, G., Allison, C.E., Böhlke, J.K., Bontempo, L., Brewer, P., Camin, F., Carter, J.F., Chartrand, M.M.G., Coplen, T.B., Gröning, M., Hélie, J., Esquivel-Hernández, G., Kraft, R.A., Magdas, D.A., Mann, J.L., Meija, J., Meijer, H.a.J., Moossen, H., Ogrinc, N., Dunn, P.J.H., 2022. Minimum requirements for publishing hydrogen, carbon, nitrogen, oxygen and sulfur stable-isotope delta results (IUPAC Technical Report). Pure Appl. Chem. 94 (11–12), 1249–1255. https://doi.org/10.1515/pac-2021-1108.

Smith, D.N., Ortega-Camacho, D., Acosta-González, G., Leal-Bautista, R.M., Fox, W.E., Cejudo, E., 2020. A multi-approach assessment of land use effects on groundwater quality in a karstic aquifer. Heliyon 6 (5), e03970. https://doi.org/10.1016/j.heliyon.2020.e03970.

Sprenger, M., Tetzlaff, D., Tunaley, C., Dick, J., Soulsby, C., 2017. Evaporation fractionation in a peatland drainage network affects stream water isotope composition. Water Resour. Res. 53, 851–866. https://doi.org/10.1002/2016wr019258.

Stein, A.F., Draxler, R.R., Rolph, G.D., Stunder, B.J.B., Cohen, M.D., Ngan, F., 2015. NOAA's HYSPLIT atmospheric transport and dispersion modeling System. Bull Amer Meteor Soc 96, 2059–2077. https://doi.org/10.1175/BAMS-D-14-00110.1.

Tarbuck, E.J., Lutgens, F.K., Tasa, D., Linneman, S., 2019. Earth: an Introduction to Physical Geology, thirteenth ed. Pearson, Hoboken, New Jersey.

Toohey, R.C., Boll, J., Brooks, E.S., Jones, J.R., 2017. Effects of land use on soil properties and hydrological processes at the point, plot, and catchment scale in volcanic soils near Turrialba, Costa Rica. Geoderma 315, 138–148. https://doi.org/10.1016/j.geoderma.2017.11.044.

Topping, J., 1972. Errors of Observation and their Treatment. Springer eBooks. https://doi.org/10.1007/978-94-011-6928-8.

Ulloa, A., Aguilar, T., Goicoechea, C., Ramírez, R., 2011. Descripción, clasificación y aspectos geológicos de las zonas kársticas de Costa Rica. Rev. Geol. Am. Cent. 45. https://doi.org/10.15517/rgac.v0i45.1910.

Wan, W., Döll, P., Schmied, H.M., 2024. Global-Scale groundwater recharge modeling is improved by tuning against ground-based estimates for Karst and non-karst areas. Water Resour. Res. 60 (3). https://doi.org/10.1029/2023wr036182.

White, W.B., 2007. Evolution and age relations of Karst landscapes. Acta Carsologica 36 (1). https://doi.org/10.3986/ac.v36i1.207.

Williams, P., 2008. The role of the epikarst in karst and cave hydrogeology: a review. Int. J. Speleol. 37 (1), 1–10. https://doi.org/10.5038/1827-806x.37.1.1.

Xiang, W., Si, B.C., Biswas, A., Li, Z., 2019. Quantifying dual recharge mechanisms in deep unsaturated zone of Chinese Loess Plateau using stable isotopes. Geoderma 337, 773–781. https://doi.org/10.1016/j.geoderma.2018.10.006.

Zhang, Z., Chen, X., Cheng, Q., Soulsby, C., 2019. Storage dynamics, hydrological connectivity and flux ages in a karst catchment: conceptual modelling using stable isotopes. Hydrol. Earth Syst. Sci. 23 (1), 51–71. https://doi.org/10.5194/hess-23-51-2019.

Zhang, H., Xu, Y., Kanyerere, T., 2020. A review of the managed aquifer recharge: historical development, current situation and perspectives. Phys. Chem. Earth, Parts A/B/C 118–119, 102887. https://doi.org/10.1016/j.pce.2020.102887.